

# An Analysis of Film Boiling around a Vertical Finite-Length Cylinder

by

Takashi YAMADA\*, Toru SHIGECHI\*,  
Satoru MOMOKI\* and Kuniyasu KANEMARU\*

The film boiling heat transfer from a vertically placed cylinder of finite-length was analyzed to predict the overall heat transfer rate around the cylinder in terms of boiling curve. The overall heat transfer rate around the cylinder was determined semi-empirically by taking into account each convective heat transfer on the bottom, side and top surfaces of the cylinder. The heat transfer rate on the bottom surface was analyzed by the method similar to that developed by the authors for a downward-facing horizontal circular plate. For the vertical lateral surface of the cylinder, Bromley's model was applied and modified to accommodate the continuity of the vapor flow rate at the lower end of the vertical surface of the cylinder, where the vapor film had a finite thickness due to the vapor inflow out of the bottom surface. Berenson's correlation was adopted on the top surface. The effects of length and diameter of the cylinder on the overall heat transfer rate were discussed in terms of boiling curve and the present prediction method was compared with the experimental data obtained by quenching method. The predicted values with the boundary condition of non-slip at the vapor-liquid interface varied within 30 percent, depending on the length and diameter of the cylinder, in terms of average wall heat flux. The prediction agreed reasonably with the experimental data.

## 1. Introduction

Film boiling heat transfer around three-dimensional bodies occurs often in such as metal quenching, manufacturing processes, emergency core cooling of nuclear reactor and so on.

A lot of studies for boiling heat transfer have been carried out in regard to metal quenching<sup>1)</sup>. However the knowledge on the boiling mechanism is insufficient. The film boiling heat transfer around the three-dimensional bodies cannot be properly predicted.

In this study, the film boiling heat transfer from a vertically placed cylinder of finite-length to a saturated liquid was semi-empirically predicted and the prediction was compared in terms of boiling curve with the experimental data obtained by quenching method. The prediction was in agreement within 30 percent with the data.

## Nomenclature

$A$	entire heating surface of the cylinder
$B$	dimensionless parameter, Eqs.(80) and (82)
$c_p$	specific heat at constant pressure
$D$	diameter of cylinder(Fig.1)
$g$	gravity acceleration
$Gr$	Grashof number
$h$	local heat transfer coefficient
$\bar{h}$	average heat transfer coefficient

$l$	latent heat
$L$	length of cylinder(Fig.1)
$\dot{m}$	mass flow rate per unit circumference, Eq.(83)
$\dot{M}$	mass flow rate, Eq.(46)
$Nu$	local Nusselt number
$\bar{Nu}$	average Nusselt number
$Pr$	Prandtl number
$q$	average wall heat flux
$Q$	total heat transfer rate
$r$	radial position(Fig.2)
$Sp$	dimensionless degree of superheating
$T$	temperature
$T_w$	wall temperature
$T_{sat}$	saturation temperature
$\Delta T_{sat}$	degree of superheating $\equiv T_w - T_{sat}$
$u$	fluid velocity
$x$	vertical position along the vertical surface(Fig.3)
$y$	position normal to the surface (Figs.2 and 3)
$\delta$	vapor film thickness
$\lambda$	thermal conductivity
$\mu$	dynamic viscosity
$\nu$	kinematic viscosity
$\rho$	density
$\sigma$	surface tension

## Superscripts

—	averaged value
---	----------------

Received on October 27, 2000

\* Department of Mechanical Systems Engineering

~ dimensionless

### Subscripts

A	horizontal bottom surface(Fig.1)
B	vertical lateral surface(Fig.1)
C	horizontal top surface(Fig.1)
L	liquid
V	vapor
sat	saturated condition
w	wall (heat transfer surface)

## 2. Analysis

A finite-length cylinder with diameter,  $D$ , and length,  $L$ , is cooled by film boiling in a saturated liquid. The temperatures inside the cylinder and of the liquid are uniform, respectively, at  $T_w$  and  $T_{sat}$ . The physical model is shown in Fig.1.

### 2.1 Total Heat Transfer Rate

The total heat transfer rate around the cylinder,  $Q$ , is predicted as

$$Q = Q_A + Q_B + Q_C \quad (1)$$

where  $Q_A$  is the heat transfer rate from the downward-facing surface(part A in Fig.1),  $Q_B$  the one from the vertical surface (part B in Fig.1) and  $Q_C$  the one from the upward-facing surface (part C in Fig.1).  $Q_A$ ,  $Q_B$  and  $Q_C$  are defined as follows:

$$Q_A \equiv \bar{h}_A(T_w - T_{sat})(\pi D^2/4) \quad (2)$$

$$Q_B \equiv \bar{h}_B(T_w - T_{sat})(\pi DL) \quad (3)$$

$$Q_C \equiv \bar{h}_C(T_w - T_{sat})(\pi D^2/4) \quad (4)$$

where  $\bar{h}$  is the heat transfer coefficient averaged on the each surface with subscript A, B or C.

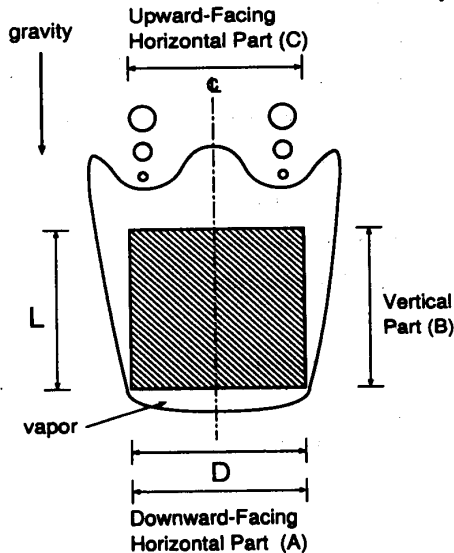


Fig. 1 Film boiling model around a vertical finite-length cylinder

The entire heating surface of the cylinder,  $A$ , is given by

$$A \equiv \pi DL + 2(\pi D^2/4) \quad (5)$$

The wall heat flux averaged on the entire heating surface of the cylinder,  $q$ , is calculated as

$$q \equiv Q/A \equiv \bar{h} \Delta T_{sat} \\ = \left[ \frac{\bar{h}_A + 4\bar{h}_B(L/D) + \bar{h}_C}{2 + 4(L/D)} \right] \Delta T_{sat} \quad (6)$$

where  $\Delta T_{sat}$  is a degree of wall superheating.

The average heat transfer coefficients in Eq.(6),  $\bar{h}_A$ ,  $\bar{h}_B$  and  $\bar{h}_C$ , are predicted below.

The common assumptions adopted for the analyses of both the downward-facing and the vertical lateral surfaces are:

1. The flow in the vapor film is incompressible and steady laminar.
2. The vapor-liquid interface is smooth and the effect of surface tension is neglected.
3. The entire surface temperature of the cylinder is constant.
4. Physical properties are constant. Physical properties for the vapor film are estimated at the average temperature of  $T_w$  and  $T_{sat}$ , i.e.  $(T_w + T_{sat})/2$ .
5. Radiation heat transfer is neglected.

In the following analysis, the subscript **A** refers to the case of the bottom surface, the subscript **B** to that of vertical lateral surface and the subscript **C** to that of the top surface.

### 2.2 Heat Transfer under the Downward-facing Surface

We already analyzed the film boiling heat transfer under the downward-facing horizontal circular plate and discussed in details on the vapor film thickness, heat transfer rate and Nusselt number<sup>2-3)</sup>. The analysis for the horizontal bottom surface similar to that for the downward-facing horizontal circular plate will be briefly described.

The physical model and coordinate system( $r_A$ ,  $y$ ) for the bottom surface(part A in Fig.1) is shown in Fig.2.

The momentum and energy equations for the vapor film are given as

$$0 = -(\rho_L - \rho_V)g \frac{d\delta_A}{dr_A} + \mu_V \frac{\partial^2 u}{\partial y^2} \quad (7)$$

$$0 = \lambda_V \frac{\partial^2 T}{\partial y^2} \quad (8)$$

The inertia and convection terms are neglected, respectively, in Eq.(7) and Eq.(8) in order to simplify the analysis. The boundary conditions are:

$$y = 0 : u = 0 \quad (9)$$

$$T = T_w \quad (10)$$

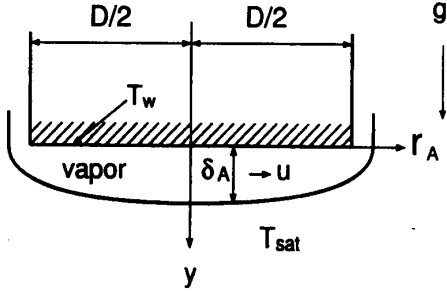


Fig. 2 Physical model and coordinate system for the bottom surface

$$y = \delta_A : T = T_{\text{sat}} \quad (11)$$

$$-\lambda_v \frac{\partial T}{\partial y} \Big|_{\delta_A} = \ell \frac{1}{r_A} \frac{d}{dr_A} \left[ \int_0^{\delta_A} r_A \rho_v u dy \right] \quad (12)$$

In this analysis, the following two kinds of boundary conditions are specified for the flow condition at the vapor-liquid interface ( $y = \delta_A$ ).

$$y = \delta_A : \begin{cases} u = 0 & \text{[CASE A-ns]} \\ \frac{\partial u}{\partial y} = 0 & \text{[CASE A-s]} \end{cases} \quad (13)$$

In Eq.(13), the boundary condition for [CASE A-ns] corresponds to the non-slip condition at the vapor-liquid interface, and the other for [CASE A-s] to the slip condition.

Solving Eq.(7) together with Eq.(9) and Eq.(13), we have

[CASE A-ns] :

$$u = \frac{1}{2} \left[ \frac{(\rho_L - \rho_v)g}{\mu_v} \delta_A^2 \frac{d\delta_A}{dr_A} \right] \left[ \left( \frac{y}{\delta_A} \right)^2 - \left( \frac{y}{\delta_A} \right) \right] \quad (14)$$

[CASE A-s] :

$$u = \frac{1}{2} \left[ \frac{(\rho_L - \rho_v)g}{\mu_v} \delta_A^2 \frac{d\delta_A}{dr_A} \right] \left[ \left( \frac{y}{\delta_A} \right)^2 - 2 \left( \frac{y}{\delta_A} \right) \right] \quad (15)$$

Also, solving Eq.(8) together with Eq.(10) and Eq.(11), we have

$$T = T_w - \Delta T_{\text{sat}} \left( \frac{y}{\delta_A} \right) \quad (16)$$

where  $\Delta T_{\text{sat}} \equiv T_w - T_{\text{sat}}$ .

Applying Eq.(14) (or Eq.(15)) and Eq.(16) to Eq.(12), we obtain the following differential equations for the vapor film thickness  $\delta_A$ .

[CASE A-ns] :

$$\frac{1}{r_A} \frac{d}{dr_A} \left[ r_A^3 \frac{d\delta_A}{dr_A} \right] = -12 \left[ \frac{\nu_v}{(\rho_L - \rho_v)g} \frac{\lambda_v \Delta T_{\text{sat}}}{\ell} \right] \frac{1}{\delta_A} \quad (17)$$

[CASE A-s] :

$$\frac{1}{r_A} \frac{d}{dr_A} \left[ r_A^3 \frac{d\delta_A}{dr_A} \right] = -3 \left[ \frac{\nu_v}{(\rho_L - \rho_v)g} \frac{\lambda_v \Delta T_{\text{sat}}}{\ell} \right] \frac{1}{\delta_A} \quad (18)$$

The boundary conditions of Eq.(17) or Eq.(18) are specified as:

$$\bar{r}_A = 0 : \frac{d\bar{\delta}_A}{d\bar{r}_A} = 0 \quad (19)$$

$$\bar{r}_A = \frac{D}{2} : \frac{d\bar{\delta}_A}{d\bar{r}_A} = -\infty \quad (20)$$

Introducing the following dimensionless variables and parameters:

$$\bar{r}_A \equiv r_A / D \quad (21)$$

$$\bar{\delta}_A \equiv (\delta_A / D) [Gr_A / Sp]^{1/5} \quad (22)$$

$$Gr_A \equiv (gD^3 / \nu_v^2) [(\rho_L / \rho_v) - 1] \quad (23)$$

$$Sp \equiv c_{p,v} \Delta T_{\text{sat}} / (Pr_v \ell) \quad (24)$$

Eq.(17) and Eq.(18) together with Eqs.(19) and (20) are transformed to

[CASE A-ns] :

$$\frac{1}{\bar{r}_A} \frac{d}{d\bar{r}_A} \left[ \bar{r}_A^3 \frac{d\bar{\delta}_A}{d\bar{r}_A} \right] = -12 \left( \frac{1}{\bar{\delta}_A} \right) \quad (25)$$

[CASE A-s] :

$$\frac{1}{\bar{r}_A} \frac{d}{d\bar{r}_A} \left[ \bar{r}_A^3 \frac{d\bar{\delta}_A}{d\bar{r}_A} \right] = -3 \left( \frac{1}{\bar{\delta}_A} \right) \quad (26)$$

The boundary conditions are:

$$\bar{r}_A = 0 : \frac{d\bar{\delta}_A}{d\bar{r}_A} = 0 \quad (27)$$

$$\bar{r}_A = \frac{1}{2} : \frac{d\bar{\delta}_A}{d\bar{r}_A} = -\infty \quad (28)$$

The differential equations given by Eqs.(25) to (28) reduce to the following second-order boundary-value problems.

[CASE A-ns] :

$$\frac{d\phi}{d\bar{r}_A} = - \left[ \left( \frac{3}{\bar{\delta}_A} \right) \phi^2 + \left( \frac{1}{\bar{r}_A} \right) \phi + \left( \frac{12}{\bar{\delta}_A^4} \right) \right] \quad (29)$$

[CASE A-s] :

$$\frac{d\phi}{d\bar{r}_A} = - \left[ \left( \frac{3}{\bar{\delta}_A} \right) \phi^2 + \left( \frac{1}{\bar{r}_A} \right) \phi + \left( \frac{3}{\bar{\delta}_A^4} \right) \right] \quad (30)$$

The function  $\phi$  in Eq.(29) and Eq.(30) is defined as

$$\phi = \frac{d\bar{\delta}_A}{d\bar{r}_A} \quad (31)$$

The boundary conditions are:

$$\bar{r}_A = 0 : \phi = 0 \quad (32)$$

$$\bar{r}_A = \frac{1}{2} : \phi = -\infty \quad (33)$$

The second-order boundary-value problems given by Eqs.(29) to (33) were solved numerically by the shooting method<sup>1)</sup>, i.e., treating the problem as an initial-value problem using assumed values of  $\bar{\delta}_A$  at  $\bar{r}_A = 0$ . The procedure was repeated until the other boundary condition of Eq.(33) was satisfied. The ordinary differential equations were solved numerically by the Runge-Kutta-Fehlberg method<sup>1)</sup>. The numerical values of  $\bar{\delta}_{A,0}$  (the value of  $\bar{\delta}_A$  at  $\bar{r}_A = 0$ ) and  $\int_0^{1/2} (\bar{r}_A / \bar{\delta}_A) d\bar{r}_A$  were determined as

[CASE A-ns]:

$$\bar{\delta}_{A,0} = 1.267795 \quad (34)$$

$$\int_0^{1/2} (\bar{r}_A / \bar{\delta}_A) d\bar{r}_A = 0.129091 \quad (35)$$

[CASE A-s]:

$$\bar{\delta}_{A,0} = 0.960797 \quad (36)$$

$$\int_0^{1/2} (\bar{r}_A / \bar{\delta}_A) d\bar{r}_A = 0.170337 \quad (37)$$

The local and average Nusselt numbers are calculated as

Local Nusselt number:

$$Nu_A \equiv \frac{h_A \cdot D}{\lambda_V} \quad (38)$$

$$h_A \equiv \lambda_V \frac{1}{\Delta T_{\text{sat}}} \left[ -\frac{\partial T}{\partial y} \Big|_0 \right] = \frac{\lambda_V}{\bar{\delta}_A} \quad (39)$$

$$Nu_A = (1/\bar{\delta}_A) [Gr_A/Sp]^{1/5} \quad (40)$$

Average Nusselt number:

[CASE A-ns]:

$$\overline{Nu}_A \equiv \frac{\overline{h}_A \cdot D}{\lambda_V} \quad (41)$$

$$\overline{h}_A \equiv \frac{4}{\pi D^2} \int_0^{D/2} h_A 2\pi r_A dr_A \quad (42)$$

$$\overline{Nu}_A = \left[ 8 \int_0^{1/2} (\bar{r}_A / \bar{\delta}_A) d\bar{r}_A \right] [Gr_A/Sp]^{1/5} \quad (43)$$

[CASE A-ns]:

$$\overline{Nu}_A = 1.0327 [Gr_A/Sp]^{1/5} \quad (44)$$

[CASE A-s]:

$$\overline{Nu}_A = 1.3627 [Gr_A/Sp]^{1/5} \quad (45)$$

The local mass flow rate of vapor at  $r_A$ ,  $\dot{M}_A$  [kg/s], is defined as

$$\dot{M}_A \equiv \int_0^{\delta_A} \rho_V u 2\pi r_A dy \quad (46)$$

Substituting  $u$  of Eq.(14) (or Eq.(15)) into Eq.(46) and applying the integral form of Eq.(17) (or Eq.(18)), we have the following relations

$$\dot{M}_A = 2\pi(\rho_V \nu_V D) [Gr_A/Sp^4]^{1/5} \int_0^{\bar{r}_A} (\bar{r}_A / \bar{\delta}_A) d\bar{r}_A \quad (47)$$

$$\dot{M}_A \Big|_{\bar{r}_A=0} = 0 \quad (48)$$

$$\dot{M}_A \Big|_{\bar{r}_A=1/2} = 2\pi(\rho_V \nu_V D) [Gr_A/Sp^4]^{1/5} \int_0^{1/2} (\bar{r}_A / \bar{\delta}_A) d\bar{r}_A \quad (49)$$

[CASE A-ns]:

$$\dot{M}_A \Big|_{\bar{r}_A=1/2} = 0.81110 (\rho_V \nu_V D) [Gr_A Sp^4]^{1/5} \quad (50)$$

[CASE A-s]:

$$\dot{M}_A \Big|_{\bar{r}_A=1/2} = 1.07026 (\rho_V \nu_V D) [Gr_A Sp^4]^{1/5} \quad (51)$$

### 2.3 Heat Transfer on the Vertical Surface

For the case of vertical surfaces Bromley's analytical treatments are well known<sup>5</sup>. Bromley treated the case that the vapor film thickness at the lower end of the vertical plate was zero. In the present study, the vapor film thickness at the lower end does not become zero because the vapor generated under the bottom surface flows upward around the corner. In the following analysis Bromley's analytical treatment is modified to accommodate the non-zero vapor film thickness at the lower end.

The physical model and coordinate system( $x_B, y$ ) for the vertical surface(part **B** in Fig.1) is shown in Fig.3. The assumptions are the same as in the analysis of the case of the horizontal bottom surface. Furthermore, in this analysis, the effect of curvature of a cylinder is neglected. That is, the vertical lateral surface of the cylinder is treated as plane surface. Thus, the application of the present study should be limited to the case of cylinders with larger diameters.

The momentum and energy equations for the vapor film are given as

$$0 = (\rho_L - \rho_V)g + \mu_V \frac{\partial^2 u}{\partial y^2} \quad (52)$$

$$0 = \lambda_V \frac{\partial^2 T}{\partial y^2} \quad (53)$$

The inertia and convection terms are neglected, respectively, in Eq.(52) and Eq.(53). The boundary conditions are:

$$y = 0 : u = 0 \quad (54)$$

$$T = T_w \quad (55)$$

$$y = \delta_B : T = T_{\text{sat}} \quad (56)$$

$$-\lambda_V \frac{\partial T}{\partial y} \Big|_{\delta_B} = \ell \frac{d}{dx_B} \left[ \int_0^{\delta_B} \rho_V u dy \right] \quad (57)$$

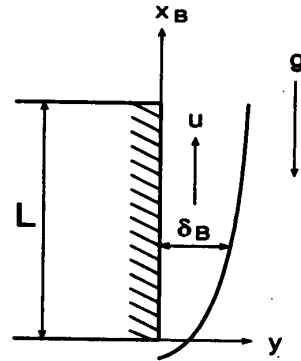


Fig. 3 Physical model and coordinate system for the vertical lateral surface

The following two kinds of boundary conditions are considered for the flow condition at the vapor-liquid interface ( $y = \delta_B$ ).

$$y = \delta_B : \begin{cases} u = 0 & \text{[CASE B-ns]} \\ \frac{\partial u}{\partial y} = 0 & \text{[CASE B-s]} \end{cases} \quad (58)$$

Solving Eq.(52) together with Eq.(54) and Eq.(58), we have

[CASE B-ns]:

$$u = \frac{1}{2} \left[ \frac{(\rho_L - \rho_V)g}{\mu_V} \delta_B^2 \right] \left[ \left( \frac{y}{\delta_B} \right) - \left( \frac{y}{\delta_B} \right)^2 \right] \quad (59)$$

[CASE B-s]:

$$u = \frac{1}{2} \left[ \frac{(\rho_L - \rho_V)g}{\mu_V} \delta_B^2 \right] \left[ 2 \left( \frac{y}{\delta_B} \right) - \left( \frac{y}{\delta_B} \right)^2 \right] \quad (60)$$

Also, solving Eq.(53) together with Eq.(55) and Eq.(56), we have

$$T = T_w - \Delta T_{\text{sat}} \left( \frac{y}{\delta_B} \right) \quad (61)$$

Applying Eq.(59) (or Eq.(60)) and Eq.(61) to Eq.(57), the following differential equations are obtained:

[CASE B-ns]:

$$\frac{d\delta_B^4}{dx_B} = 16 \left[ \frac{\nu_V}{(\rho_L - \rho_V)g} \frac{\lambda_V \Delta T_{\text{sat}}}{\ell} \right] \quad (62)$$

[CASE B-s]:

$$\frac{d\delta_B^4}{dx_B} = 4 \left[ \frac{\nu_V}{(\rho_L - \rho_V)g} \frac{\lambda_V \Delta T_{\text{sat}}}{\ell} \right] \quad (63)$$

Introducing the following dimensionless variables and parameters:

$$\tilde{x}_B \equiv x_B/L \quad (64)$$

$$\tilde{\delta}_B \equiv (\delta_B/L) [Gr_B/Sp]^{1/4} \quad (65)$$

$$Gr_B \equiv (gL^3/\nu_V^2) [(q/\rho_V) - 1] \quad (66)$$

$$Sp \equiv q_{\nu_V} \Delta T_{\text{sat}} / (Pr_V \ell) \quad (67)$$

Eq.(62) and Eq.(63) are transformed to

[CASE B-ns]:

$$\frac{d\tilde{\delta}_B^4}{d\tilde{x}_B} = 16 \quad (68)$$

[CASE B-s]:

$$\frac{d\tilde{\delta}_B^4}{d\tilde{x}_B} = 4 \quad (69)$$

Solving Eq.(68) (or Eq.(69)) together with the initial condition:

$$\tilde{x}_B = 0 : \tilde{\delta}_B = \tilde{\delta}_{B,0} \quad (70)$$

the exact solutions for  $\tilde{\delta}_B$  are obtained as

[CASE B-ns]:

$$\tilde{\delta}_B = [16\tilde{x}_B + \tilde{\delta}_{B,0}^4]^{1/4} = 2[\tilde{x}_B + (\tilde{\delta}_{B,0}/2)^4]^{1/4} \quad (71)$$

[CASE B-s]:

$$\tilde{\delta}_B = [4\tilde{x}_B + \tilde{\delta}_{B,0}^4]^{1/4} = \sqrt{2}[\tilde{x}_B + (\tilde{\delta}_{B,0}/\sqrt{2})^4]^{1/4} \quad (72)$$

where  $\tilde{\delta}_{B,0}$ , the values of  $\tilde{\delta}_B$  at  $\tilde{x}_B = 0$ , will be determined below from the continuity of the vapor flow rate around the lower corner of the vertical cylinder.

The local and average Nusselt numbers are calculated as

Local Nusselt number :

$$Nu_B \equiv \frac{h_B \cdot L}{\lambda_V} \quad (73)$$

$$h_B \equiv \lambda_V \frac{1}{\Delta T_{\text{sat}}} \left[ -\frac{\partial T}{\partial y} \right]_0 = \frac{\lambda_V}{\delta_B} \quad (74)$$

$$Nu_B = (1/\tilde{\delta}_B) [Gr_B/Sp]^{1/4} \quad (75)$$

Average Nusselt number :

$$\overline{Nu}_B \equiv \frac{\overline{h}_B \cdot L}{\lambda_V} \quad (76)$$

$$\overline{h}_B \equiv \frac{1}{L} \int_0^L h_B dx_B \quad (77)$$

$$\overline{Nu}_B = \left[ \int_0^1 (1/\tilde{\delta}_B) d\tilde{x}_B \right] [Gr_B/Sp]^{1/4} \quad (78)$$

[CASE B-ns]:

$$\overline{Nu}_B = \frac{2}{3} [(1+B)^{3/4} - B^{3/4}] [Gr_B/Sp]^{1/4} \quad (79)$$

$$B \equiv (\tilde{\delta}_{B,0}/2)^4 \quad (80)$$

[CASE B-s]:

$$\overline{Nu}_B = \frac{2\sqrt{2}}{3} [(1+B)^{3/4} - B^{3/4}] [Gr_B/Sp]^{1/4} \quad (81)$$

$$B \equiv (\tilde{\delta}_{B,0}/\sqrt{2})^4 \quad (82)$$

where  $B$  is a dimensionless parameter which is determined from the continuity of the vapor flow rate at the lower end of the vertical surface, i.e., at the lower corner of the cylinder.

Incidentally,  $B$  is zero for the zero vapor film thickness at the lower end.

The vapor mass flow rate per unit circumference,  $\dot{m}_B$  [kg/(m·s)], is defined as

$$\dot{m}_B \equiv \int_0^{\delta_B} \rho_V u dy \quad (83)$$

$\dot{m}_B$  is calculated using Eq.(59) (or Eq.(60)) as

[CASE B-ns]:

$$\dot{m}_B = \frac{1}{12} \left[ \frac{(\rho_L - \rho_V)g}{\nu_V} \right] \delta_B^3 \quad (84)$$

[CASE B-s]:

$$\dot{m}_B = \frac{1}{3} \left[ \frac{(\rho_L - \rho_V)g}{\nu_V} \right] \delta_B^3 \quad (85)$$

Table 1 Four combinations of the boundary conditions for the bottom and side surfaces

type	boundary conditions
case 1	[CASE (A-ns + B-ns)]
case 2	[CASE (A-ns + B-s)]
case 3	[CASE (A-s + B-ns)]
case 4	[CASE (A-s + B-s)]

The value of  $\tilde{\delta}_{B,0}$  is determined from the continuity condition of vapor mass flow rate around the lower corner of the cylinder ( $\tilde{r}_A=1/2$ , i.e., at  $\tilde{x}_B=0$ ),

$$\dot{M}_A \Big|_{\tilde{r}_A=1/2} = \dot{m}_B \Big|_{\tilde{x}_B=0} \times \pi D \quad (86)$$

Applying  $\dot{M}_A$  of Eq.(50) (or Eq.(51)) and  $\dot{m}_B$  of Eq.(84) (or Eq.(85)) to Eq.(86),  $\tilde{\delta}_{B,0}$  and  $B$  are determined for the four combinations of [CASE A-ns], [CASE A-s], [CASE B-ns] and [CASE B-s] as follows:

[CASE A-ns+CASE B-ns]:

$$\tilde{\delta}_{B,0} = 1.45781 [D/L]^{1/5} [Sp/Gr_B]^{1/60} \quad (87)$$

$$B = 0.28228 [D/L]^{4/5} [Sp/Gr_B]^{1/15} \quad (88)$$

[CASE A-ns+CASE B-s]:

$$\tilde{\delta}_{B,0} = 0.91837 [D/L]^{1/5} [Sp/Gr_B]^{1/60} \quad (89)$$

$$B = 0.17783 [D/L]^{4/5} [Sp/Gr_B]^{1/15} \quad (90)$$

[CASE A-s+CASE B-ns]:

$$\tilde{\delta}_{B,0} = 1.59897 [D/L]^{1/5} [Sp/Gr_B]^{1/60} \quad (91)$$

$$B = 0.40855 [D/L]^{4/5} [Sp/Gr_B]^{1/15} \quad (92)$$

[CASE A-s+CASE B-s]:

$$\tilde{\delta}_{B,0} = 1.00729 [D/L]^{1/5} [Sp/Gr_B]^{1/60} \quad (93)$$

$$B = 0.25737 [D/L]^{4/5} [Sp/Gr_B]^{1/15} \quad (94)$$

Finally, we can estimate the magnitude of the average Nusselt number,  $\overline{Nu}_B$ , on the vertical lateral surface using Eq.(79) or Eq.(81) through the value of  $B$  calculated by Eq.(88), Eq.(90), Eq.(92) or Eq.(94) for the four cases of [CASE A-ns+CASE B-ns],[CASE A-ns+CASE B-s],[CASE A-s+CASE B-ns] and [CASE A-s+CASE B-s].

## 2.4 Heat Transfer on the Upward-facing Surface

Nusselt number on the upward-facing surface,  $\overline{Nu}_C$ , is estimated by applying the Berenson's correlation<sup>6)</sup>.

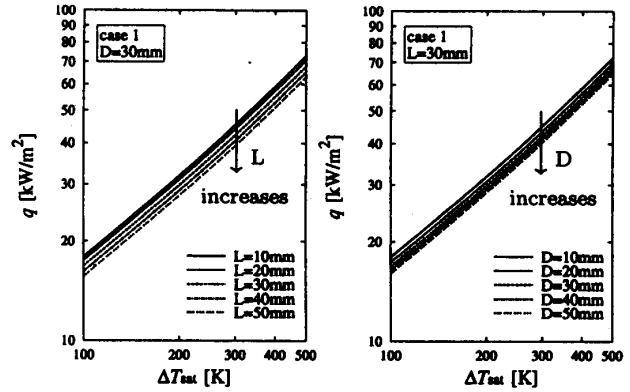
$$\overline{Nu}_C = 0.425 [Gr_C/Sp]^{1/4} \quad (95)$$

where

$$\overline{Nu}_C \equiv \overline{h}_C \cdot \lambda_0 / \lambda_v \quad (96)$$

$$Gr_C \equiv (g \lambda_0^3 / \nu_v^2) [(\rho_L / \rho_v) - 1] \quad (97)$$

$$\lambda_0 \equiv [\sigma / (g(\rho_L - \rho_{v, sat}))]^{1/2} \quad (98)$$



(a) effect of length (b) effect of diameter  
Fig.4 Effects of length and diameter on  $q$  predicted by Eq. (6) with case 1

Since the reference length of  $\overline{Nu}_C$  and  $Gr_C$  is a capillary length,  $\lambda_0$ ,  $\overline{Nu}_C$  and  $Gr_C$  are independent of the diameter of the cylinder. In Eq.(98)  $\rho_{v, sat}$  is the density of saturated vapor and  $\sigma$  is surface tension.

## 2.1 Effects of length and diameter on boiling curves

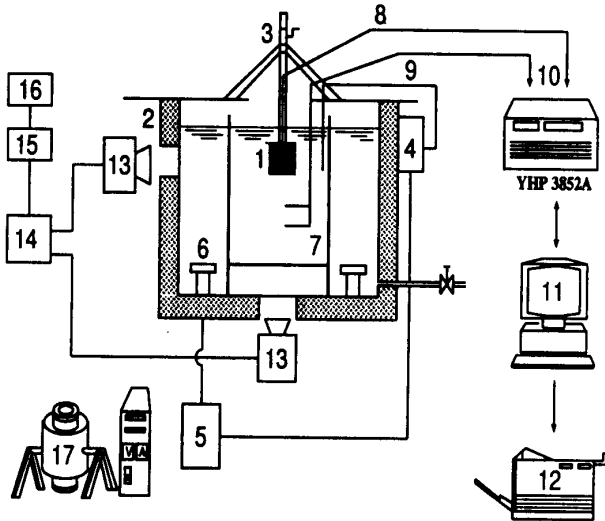
Figure 4 shows the effects of length and diameter on the average heat flux predicted by Eq.(6) with case 1. The case 1 has non-slip condition at the vapor-liquid interface for bottom and side surfaces of cylinder. These figures show that the average heat flux predicted in this analysis decreases with increasing in diameter or length. This is attributed to that the Bromley-type solution is adopted for the vertical surface and that the heat transfer on the bottom surface is smaller than on the side and top surface. Additionally, for the other combination, cases 2, 3 and 4 (see Table 1), similar tendency to case 1 is seen.

## 3. Experiments

### 3.1 Experimental Apparatus and Procedure

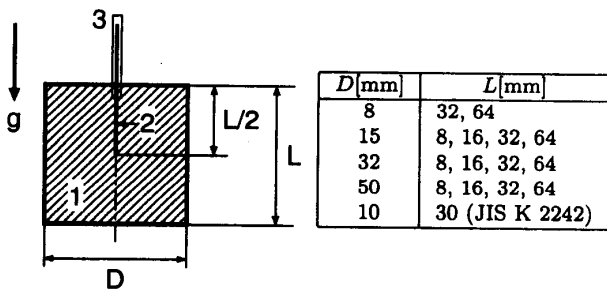
The experimental apparatus is shown in Fig.5. The experiment for film boiling around the vertical cylinder was carried out by quenching method in quiescent saturated water at atmospheric pressure.

The experimental setup employed in this study consisted of five major parts: a boiling tank, a lifting/submerging device, an electric furnace for the heating cylinder, a visual observation/photographing/videotaping system and a data acquisition system. The boiling tank with the dimensions of 450mm×450mm×750mm was made of stainless steel, and its side and bottom surfaces have four viewing windows. Water in the tank was heated up by two 2000W immersion



1. Test cylinder 2. Boiling bath 3. Lifting device 4. Temperature controller 5. Power controller 6. Heater 7. Glass box 8. K type thermocouple 9. K type thermocouple 10. Data acquisition/control unit 11. Personal computer 12. Printer 13. Video camera 14. Video cassette recorder 15. Digital AV mixer 16. Video monitor 17. Electric furnace

Fig.5 Schematic of experimental apparatus



1. Silver cylinder(99.99% purity)  
 2. K-type sheath thermocouple(φ 1mm)  
 3. Supporting stainless(φ 3mm × φ 2mm)

Fig.6 Test cylinder

heaters placed at the bottom of the tank. The electric power input to these heaters was controlled by a power regulator. A glass vessel with 300mm×300mm×600mm was placed inside the tank to maintain the water stagnant, i.e., not to be disturbed by bubbles generated by the two heaters. During the experiment, the water in the tank was maintained at nearly saturated condition by a temperature controller. The test cylinders are made of silver with 99.99% purity to prevent surface oxidizing and to have high thermal conductivity.

The test cylinder is shown in Fig.6. Fifteen kinds of test

cylinders are used in this study where the diameter is 8, 15, 32 or 50 mm and the length is 8, 16, 32 or 64 mm. In addition, the cylinder with 10mm in diameter and 30mm in length is used. This is the same size as used in the cooling curves performance test of JIS K 2242 heat treating oils<sup>7)</sup>.

One type-K sheath thermocouple of 1mm diameter was inserted through the thermocouple hole drilled into its center from the upper surface of the cylinder. The temperature history of the test cylinder is monitored. The data of temperature are measured by a personal computer through the 3852A data acquisition/control unit of Yokogawa Hewlett Packard.

Prior to each test, the test cylinders were polished with diamond compound and then cleaned with ethyl alcohol to maintain the surface condition of the test cylinder constant. The test cylinder was heated to about 600°C in the electric furnace and then submerged slowly into water to the constant depth of 100mm by using the lifting/submerging device. The temperature history of cylinder during quenching was measured with sampling times of 0.25sec and 1.0sec depending on the heat capacity of cylinder (i.e., the dimension of the cylinder). The boiling phenomenon around a finite-length vertical cylinder during quenching was observed by a high speed video camera and still photopgraphing.

### 3.2 Measurements of Wall Temperature and Wall Heat Flux

The cylinder can be treated as a lumped parameter system due to small Biot number estimated to be less than 0.03 for this system. Furthermore, the assumption of the uniform temperature in the cylinder is confirmed by solving numerically the unsteady-state two-dimensional heat conduction in the cylinder. Thus, the wall heat flux averaged over the entire surface of the cylinder,  $q$ , is calculated as

$$q = -\rho c \frac{V}{A} \frac{dT}{d\tau} \quad (99)$$

where  $\rho$  is the density,  $c$  the specific heat capacity,  $V$  the volume of the cylinder,  $A$  the entire heating surface of the cylinder,  $T$  the temperature of the cylinder,  $\tau$  the time and  $dT/d\tau$  the cooling rate.

The heat loss owing to heat conduction through the supporting stainless tube was estimated to be 2 percent.

### 3.3 Cooling Curves

The cooling curves obtained for the case  $D=32$ mm and  $L=32$ mm are shown in Fig.7. The ordinate is taken to non-

dimensional temperature, as the initial temperature of the cylinder,  $T_i$ , was slightly different at each run.  $T_\infty$  is the temperature of the working fluid, i. e., the saturation temperature of water at atmospheric pressure. Fig.7(a) shows the effect of length on the temperature-history for the cooling cylinder. Fig.7(b) shows the effect of diameter on the temperature-history for the cooling cylinder. From the figures, it is seen that the cooling time was longer as the length and the diameter of the cylinder was larger. In the figures, the solid circle shows the lowest limit of film boiling where the cooling rate,  $dT/d\tau$ , becomes minimum.

### 3.4 Boiling Curves

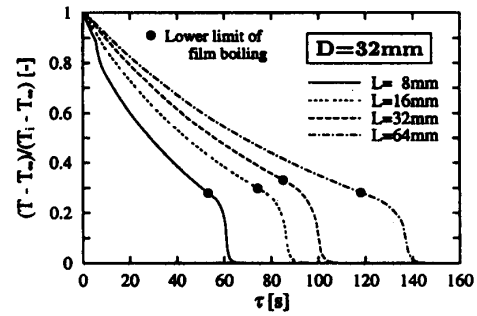
Figure 8 shows the effects of length and diameter on the average heat flux obtained by Eq.(99). From the figures, it is seen that the average heat flux increases with an increase in length and decreases with an increase in diameter. The effect of the diameter on boiling curve agrees qualitatively with the prediction. The vapor-liquid interface at the vertical surface of the cylinder becomes rough and wavy except near the lower end of vertical surface with an increase in length of the cylinder. Thus, as the length of cylinder increases, the average heat flux increases due to heat transfer enhancement on the vertical surface. In the figure, the solid circle shows the minimum heat flux point which corresponds to the same symbols in Fig.7. Table 2 shows the minimum heat flux and minimum film boiling superheat determined from the cooling curve.  $q_{\min}$  is the minimum heat flux in  $\text{kW/m}^2$  and  $\Delta T_{\text{sat}, \min}$  is the minimum film boiling superheat in K.

### 4. Comparison of Prediction with Experimental Data

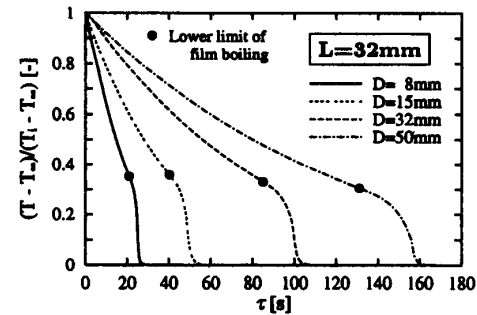
The comparisons of the prediction given by Eq.(6) with the experimental data obtained by Eq.(99) are shown in Fig.9. In the figure, the solid circle is the minimum heat flux point and these numerical values are shown in Table 2.

In the chapter 2, two kinds of Nusselt numbers were, respectively, given for the downward-facing and vertical surfaces, depending on the velocity boundary condition at the vapor-liquid interface, i.e., non-slip condition (referred to as -ns) and slip condition (referred to as -s). The four combinations (referred to as case 1, case 2, case 3 and case 4) of Nusselt number are shown in Table 1.

The Nusselt number of the upward-facing surface for the four cases is calculated by Berenson's correlation, Eq.(96).

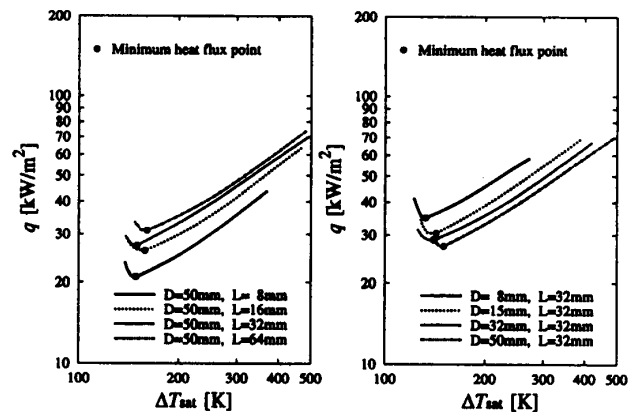


(a) effect of length



(b) effect of diameter

Fig.7 Effects of length and diameter on cooling curve



(a) effect of length

(b) effect of diameter

Fig.8 Effects of length and diameter on boiling curve based on the experimental data

Table 2 Minimum heat flux,  $q_{\min}$  [ $\text{kW/m}^2$ ] and minimum film boiling superheat,  $\Delta T_{\text{sat}, \min}$  [K]

L mm	D [mm]				
	8	15	32	50	
8	-	33.3	21.5	20.9	$q_{\min}$
	-	137.3	125.3	148.5	$\Delta T_{\text{sat}, \min}$
16	-	30.1	24.5	26.0	$q_{\min}$
	-	133.5	135.2	158.3	$\Delta T_{\text{sat}, \min}$
32	34.9	30.5	28.7	27.2	$q_{\min}$
	132.5	142.4	140.2	150.0	$\Delta T_{\text{sat}, \min}$
64	32.1	30.3	27.4	31.0	$q_{\min}$
	142.2	136.4	136.1	160.6	$\Delta T_{\text{sat}, \min}$

$D = 10\text{mm}, L = 30\text{mm} :$   
 $q_{\min} = 34.6 [\text{kW/m}^2], \Delta T_{\text{sat}, \min} = 134.5 [\text{K}]$

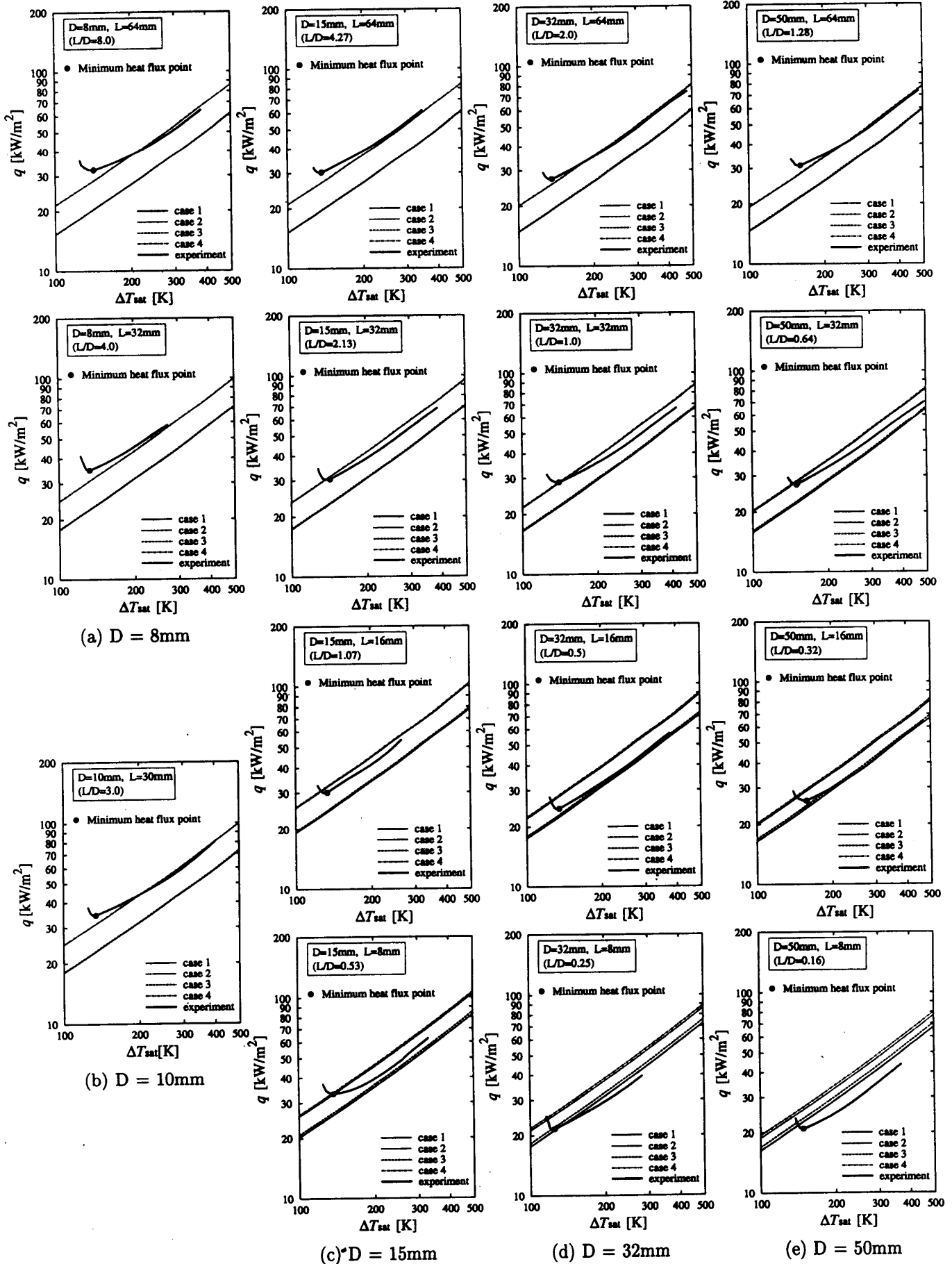


Fig.9 Comparison of semi-empirical prediction with quenching data

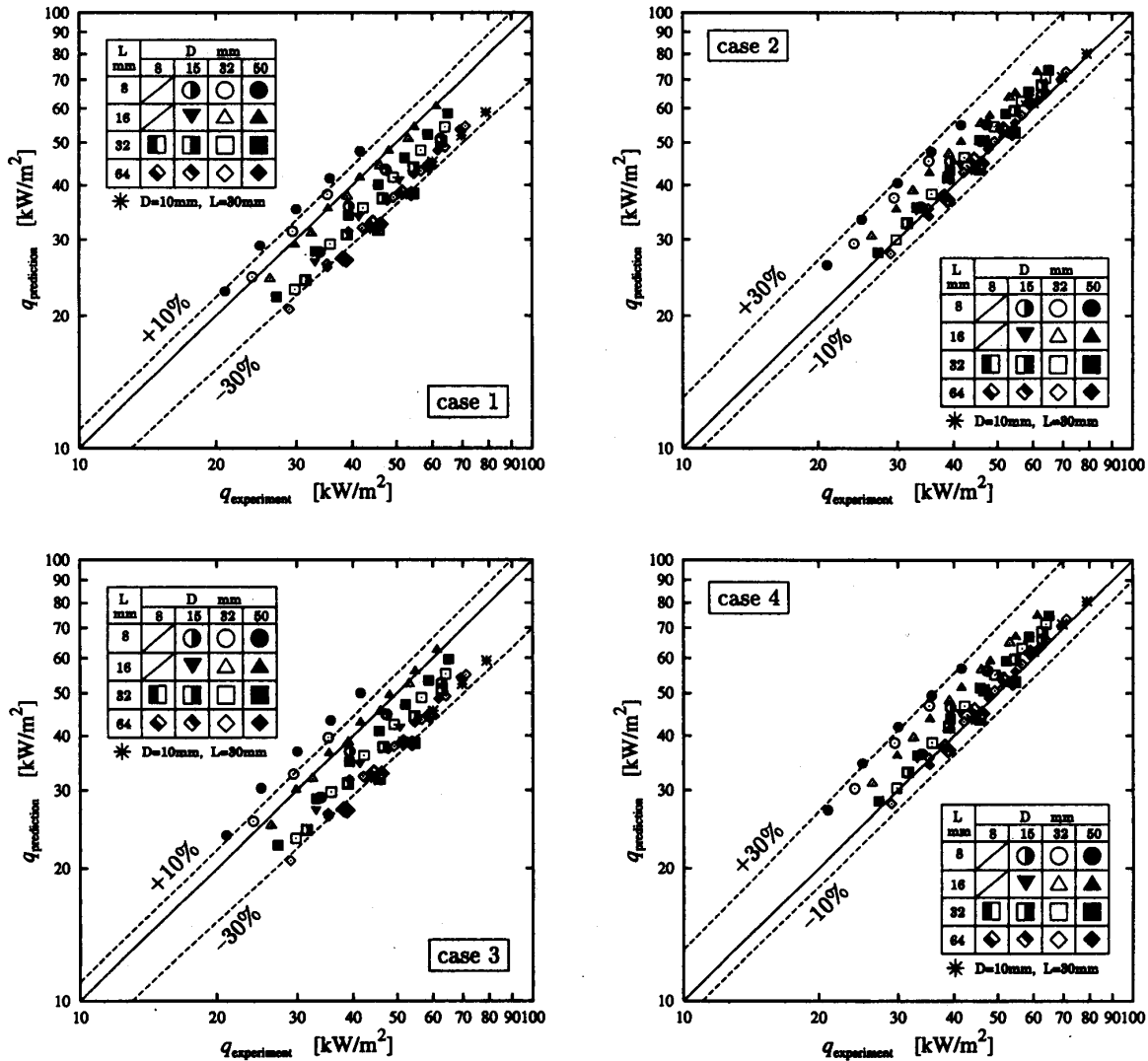


Fig.10 Relationship between semi-empirical prediction and quenching data

The prediction by the four cases gives roughly 30 % different values of average wall heat flux,  $q$ , between the highest value for case 4 and the lowest value for case 1, as shown in Fig.9. All the experimental data exist near the highest values (case 4) or lowest values (case 1).

The relationship between semi-empirical predictions for four combinations and all the experimental data are shown in Fig.10. The abscissa is the average heat flux based on the experimental data and the ordinate is the average heat flux based on the prediction. The predictions of case 1 and case 3 can predict all the experimental data within +10% to -30%. The other predictions of case 2 and case 4 can predict all the experimental data within +30% to -10%. The predictions show the tendency that in the case of small aspect ratio,  $L/D$ , the experimental data are underestimated but in the case of large aspect ratio,  $L/D$ , the experimental data are overestimated. As shown in Fig.4, this is attributed to that the

Bromley-type solution is adopted for the vertical surface, increasing the vapor film thickness of vertical surface with an increasing length of cylinder and the heat transfer rate is reduced.

## 5. Conclusions

The film boiling heat transfer from a vertical cylinder of finite-length to saturated liquids was semi-empirically analyzed. The heat transfer rate on the bottom surface was analyzed by the method similar to that developed by the authors for a downward-facing horizontal circular plate. For the vertical lateral surface of the cylinder, Bromley's model was applied and modified to accommodate the continuity of vapor mass flow rate around the lower corner of the vertical cylinder. Bereson's correlation was adopted on the top surface. The total heat transfer rate around the cylinder was determined by taking into account each convective heat

transfer on the bottom, side and top surfaces of the cylinder. The average heat flux on the vertical finite-length cylinder predicted in this analysis decreases with an increase in diameter or length of the cylinder. All the experimental data obtained by the quenching method can be correlated within 30 percent by the present prediction method.

### References

1. The Japan Society of Mechanical Engineers, Boiling Heat Transfer and Cooling(in Japanese), (1989), pp.128-143.
2. Shigechi, T., Kawae, N., Tokita, Y. and Yamada, T.; JSME International Journal, Vol.32, No.4, (1989), pp.646-651.
3. Shigechi, T., Yamada, T., Momoki, S., Kanemaru, K. and Yamaguchi, T.; Proceedings of the 5th ASME/JSME Thermal Engineering Joint Conference, (1999), CD-ROM.
4. Gerald, C.F. & Wheatley, P.O.; Applied Numerical Analysis, Third Edition, (1984), pp.310-311 and pp. 371-373.
5. Bromley, L.A.; Chem. Eng. Prog., Vol.46, No.5, (1950), pp.221-227.
6. Berenson, P.J.; Trans. ASME, J. Heat Transfer, Vol.83, (1961), pp.351-358.
7. Japanese Industrial Standards Committee, Japanese Industrial Standard, (JIS K 2242) (in Japanese), (1991).